OPEN ACCESS

University of Dundee

University of Dundee

# Small-Scale Modeling of Thermomechanical Behavior of Reinforced Concrete Energy Piles in Soil

Zhao, Rui; Leung, Anthony Kwan; Vitali, Davide; Knappett, Jonathan Adam; Zhou, Zheng

*Published in:*
Journal of Geotechnical and Geoenvironmental Engineering

*DOI:*
10.1061/(ASCE)GT.1943-5606.0002225

*Publication date:*
2020

*Document Version*
Peer reviewed version

Link to publication in Discovery Research Portal

*Citation for published version (APA):*
Zhao, R., Leung, A. K., Vitali, D., Knappett, J. A., & Zhou, Z. (2020). Small-Scale Modeling of Thermomechanical Behavior of Reinforced Concrete Energy Piles in Soil. *Journal of Geotechnical and Geoenvironmental Engineering*, *146*(4), [04020011]. https://doi.org/10.1061/(ASCE)GT.1943-5606.0002225

**General rights**
Copyright and moral rights for the publications made accessible in Discovery Research Portal are retained by the authors and/or other copyright owners and it is a condition of accessing publications that users recognise and abide by the legal requirements associated with these rights.

• Users may download and print one copy of any publication from Discovery Research Portal for the purpose of private study or research.
• You may not further distribute the material or use it for any profit-making activity or commercial gain.
• You may freely distribute the URL identifying the publication in the public portal.

**Take down policy**
If you believe that this document breaches copyright please contact us providing details, and we will remove access to the work immediately and investigate your claim.

Download date: 04. May. 2023

# Small-Scale Modelling of Thermomechanical Behavior of Reinforced Concrete Energy Piles in Soil

Rui Zhao; Anthony Kwan Leung; Davide Vitali; Jonathan Adam Knappett and Zheng Zhou

**Abstract:** Small-scale physical model tests have been increasingly used to study the thermomechanical soil-pile interaction, but existing model piles are highly simplified and do not have representative thermal properties or the quasi-brittle mechanical behavior of reinforced concrete (RC). This study aims to overcome these shortcomings by presenting a new type of model RC. This consists of a mortar (plaster, sand and water) with copper powder added to tune the mixture's thermal properties, along with a steel reinforcing cage. Fine sand was used to represent geometrical scaling of the prototype aggregates to correctly capture quasi-brittle structural response. Adding copper powder content of 6% (by volume) matched the coefficient of thermal expansion and thermal conductivity of prototype concrete, without changing the axial and flexural properties of model piles. In 1-g soil-structure interaction tests, the model pile was able to serve as an effective heat exchanger for transferring heat from a water-carrying pipe embedded within the mortar to the surrounding soil. The model RC exhibited cyclic pile head settlement due to repeated pile heating/cooling.

## Introduction

Energy piles have been increasingly used in urban spaces as heat exchangers for not only providing structural support to the superstructure above but also exploiting the renewable near-

This material may be downloaded for personal use only. Any other use requires prior permission of the American Society of Civil Engineers. This material may be found at https://dx.doi.org/10.1061/(ASCE)GT.1943-5606.0002225.

surface geothermal energy for heating, ventilation and air conditioning purposes via a ground-source heat pump (Brandl, 2006). Energy piles are typically made of reinforced concrete (RC), with pipe loops being attached to the reinforcement cage for circulating heat-carrying fluid to facilitate soil-concrete-pipe heat transfer. The alternate summer and winter operation of an energy pile continually heats and cools the pile and the surrounding soil. Cyclic pile heating and cooling mobilizes soil stress and strain (Ng et al., 2015; Stewart and McCartney, 2014; Rotta Loria and Laloui, 2016; Zhao et al., 2017; El Zeiny et al. 2018; Xiao et al. 2018), consequently affecting the pile capacity and settlement. Understanding the behavior of thermo-active pile requires improved understanding of the load transfer mechanisms due to cyclic thermal loads and thermomechanical soil responses.

Thermomechanical soil-pile interaction has been studied by different methods, namely field tests (e.g., Mimouni and Laloui, 2015; Bourne-Webb et al., 2009; Murphy and McCartney, 2015), numerical modelling (e.g., Rotta Loria and Laloui, 2016; Rotta Loria et al., 2015; Chen and McCartney, 2017; Zhao et al., 2017) and more recently, centrifuge modelling (McCartney and Rosenberg, 2011; Ng et al., 2015; Goode and McCartney, 2015; Stewart and McCartney, 2014). Centrifuge modelling enables small-scale physical models to be tested within an elevated gravity field, such that soil stress levels are identical to those experienced by much larger prototypes at homologous points and under much more controlled test conditions than are possible in field tests. A challenge to study the soil-energy pile interaction meaningfully using a centrifuge is to select an appropriate model of the pile that can simultaneously scale both the thermal and mechanical properties of the structure at prototype scale. Aluminum alloy and concrete are the two common choices of model material. For instances, Ng et al. (2015) and Yavari et al. (2014)

modelled their piles using an elastic aluminum alloy. However, only either stiffness or strength can be scaled, but not both, due to the differences in intrinsic properties between aluminum and RC (see Knappett et al., 2011). Another limitation of using this approach is its inability to capture the thermal pile behavior. The coefficient of thermal expansion (CTE) of aluminum (22.2 x $10^{-6}$ με/$^{o}$C) is up to three times higher than that of RC (6 to 9 x $10^{-6}$ με/$^{o}$C; Bourne-Webb et al., 2009), while the thermal conductivity of aluminum (205 W/m·K) is 100 – 200 times higher than that of RC (~ 1 W/m·K; GSHP, 2012). This mismatch of model and prototype thermal properties means that aluminum alloy is unable to study the efficiency of pipe-concrete-soil heat transfer properly.

Reinforced concrete has been used (e.g., Stewart and McCartney, 2014) as an option to model the thermomechanical behavior of energy piles. Although the thermal properties in this case are more realistically modelled, the particle size of coarse aggregates in the RC does not scale geometrically. This means that the particle size distribution is the same between the model and prototype scale, which would potentially result in over-strength of the model material (e.g. Belgin and Sener, 2008). Proper scaling of the particle size in a RC model is crucial for correctly capturing the failure mechanism and the cracking process of this kind of quasi-brittle and non-linear material (Bažant, 2005). To overcome this shortcoming, attempts have been made to use plaster-based mortars to capture the quasi-brittleness of RC. Knappett et al. (2011) created various types of mortar, in which fine silica sand is used to geometrically scale the coarse aggregate in RC. This type of model concrete mimicked the nonlinear quasi-brittle behavior of concrete and has representative mechanical strengths (i.e. unconfined compressive strength from 26.3 to 81.7 MPa and modulus of rupture from 2.02 to 4.42 MPa). These types of model concrete have been successfully used for modelling various non-energy structural elements in centrifuge tests,

including pile-reinforced slopes (Al-Defae and Knappett, 2014) and RC bridge piers on rocking shallow foundations (Loli et al., 2014).

This study aims to build on this previous work, developing a new model RC that is thermally enhanced to more realistically scale the thermomechanical properties of RC energy pile representative to those in prototype. A series of structural tests was undertaken to characterize the thermal, mechanical and coupled thermomechanical properties of the model RC. To illustrate the capabilities of the new model RC, it was used to construct model energy piles for evaluating their axial thermomechanical interaction in soil at 1-g.

## New model concrete

### *Constituents of the new model concrete*

The new model concrete is based on the plaster-based mortars pioneered by Knappett et al. (2011). Their model concrete composes of either $\alpha$-form dental stone or $\beta$-form surgical plaster, water and silica sand (Congleton HST95). To enhance the thermal properties of their mix for modelling the behavior of energy piles, copper powder (Phoenix Scientific Industries) was incorporated into the mix. Copper powder has a much higher thermal conductivity (400 W/m·K) than plaster (0.29 W/m·K) and quartz (i.e. 6.5 W/m·K). The diameter of the copper powder used ranges from 0.002 to 0.1 mm, and the $D_{10}$ (the particle diameter at 10% passing), $D_{30}$ and $D_{60}$ are 0.013, 0.026 and 0.042 mm, respectively. The 'mix 2' design mix from Knappett et al. (2011) was adopted here. This utilizes $\beta$-form surgical plaster at a water/plaster ratio of 0.9:1 and sand/plaster ratio of 1:1, to which various amounts of copper powder were added. The mix was left air-cured at room temperature (20 – 24 °C) for 28 days prior to testing.

***Thermal and mechanical behavior***

A series of tests were conducted to characterize the thermal properties of the new model concrete and to study whether the addition of copper power might affect the fundamental mechanical properties. Thermal conductivity tests were performed on slab samples (45 mm x 150 mm x 150 mm) by using a hot box apparatus. Three copper powder contents (0, 6 and 12% by volume) were considered. Three replications were tested for each mix. Following BS 874-3.2:1990, each specimen was subjected to a controlled heat gradient across its thickness and heat flux was measured. By Fourier's law, the thermal conductivity was determined. As expected, adding a more thermally conductive material (i.e. copper powder) into the mix increased the thermal conductivity of the model concrete from 0.38±0.01 to 0.73±0.08 and then to 0.94±0.04 W/(m K) (mean ± standard error of mean) as the copper powder content increased from 0%, 6% to 12%, respectively. Comparing with the values for concrete typically used to construct energy piles (1 – 4 W/(m K); GSHP, 2012), copper powder contents ranging from 6 to 12% are deemed appropriate for capturing the thermal properties of energy piles.

Unconfined compression tests (BS EN 12390-3:2009) were conducted. Cubic samples (100 mm) were tested for compressive strength ($f_{c,100}$) with three replications for each copper powder content. The mean strength of 6% copper powder normalized by that of the non-thermal model concrete (0% copper) is 1.00±0.37. One-way analysis of variance (ANOVA) showed that the normalized strength between 0% and 6% cases are statistically not different ($p$-value = 0.592 > 0.05). This means that the addition of copper powder did not adversely affect the compressive strength of the new model concrete.

Effects of copper powder on the modulus of rupture of the new model concrete were also

determined via four-point bending (FPB) tests, following BS EN 12390-5:2009. Six replications of beam samples (25 mm x 25 mm x 250 mm) were tested for each copper powder content. The modulus of rupture for 6% and 12% copper powder, normalized by the value obtained at 0%, was 1.06±0.02 and 1.08±0.14, respectively. As above, ANOVA suggests a *p*-value of 0.143 (> 0.05), meaning that there is no statistically-significant difference between these tests. This suggests that the addition of copper power did not substantially affect the modulus of rupture.

**Design of model RC energy piles**

Having assessed the fundamental thermal and mechanical properties of the model concrete, it was subsequently used to produce small-scale model RC energy piles, designed for future centrifuge model tests following the 'high-g' scaling laws summarized in Table 1. Two types of piles were considered, one for testing axial behavior and the other for flexural behavior.

The first pile type is a 1:35$^{th}$ model energy pile (type 1) designed as a part of a tall building foundation, which means that the pile was expected to be subject to both axial and lateral loading at the pile head. Considering the physical constraints of the model size, a pile geometry of 0.63 m x 0.63 m x 10.5 m (in prototype) was chosen. Following Broms (1964), this pile geometry would necessitate a design moment capacity of approximately 200 kNm in sandy soil (friction angle of 32$^{o}$), which matches the range of typical values found in the literature (e.g., Al-Defae and Knappett 2014; Hayward et al. 2000). Following Eurocode 2 (EN 1992-1-1, 2004), four longitudinal steel bars of 35 mm diameter each and 10 shear links of 22 mm diameter each with 1.05 m spacing are needed (Fig. 1). The longitudinal reinforcement ratio is 1.0%. Both scaled longitudinal bars and shear links were made of stainless steel wire (Grade 316; Ormiston Wire Ltd), which has

a CTE of 18.5 με/°C. Stainless steel with a yield strength of 460 MPa and a model diameter of 1 mm was used for producing the longitudinal bars, while that with a yield strength of 380 MPa and a model diameter of 0.6 mm was adopted for producing the shear links. All reinforcement was coated with fine sand using epoxy for providing mechanical interlocking with the mortar (after Knappett et al., 2011).

To allow heat energy to be circulated in and out of the model energy piles, two flexible silicone pipes with a model internal diameter of 1.5 mm each were used. The silicone pipe has a tensile strength of 10 MPa and the CTE ranges from 70 to 110 με/◦C. Each pipe was attached to shear links between the longitudinal bars with a few spots of rapid-set glue forming a U-shape loop arrangement as shown in Fig. 1, as commonly adopted in the field (e.g. Loveridge and Powrie, 2013; Mimouni and Laloui, 2015). The longitudinal bars, shear links and the two U-shaped silicone piles were assembled in a multi-part formwork, into which the mortar mix with 6% copper powder was poured and subsequently air-cured for 28 days.

The second pile type is a 1:24$^{th}$ model pile designed as part of a discretely-spaced pile row for slope stabilization, and thus it would be subjected to predominately lateral loading. According to the test results of non-energy pile reinforcement systems reported by Al-Defae and Knappett (2014) and Jeong et al. (2003), a mean pile moment capacity of 230 kNm was used as a design value. Following Eurocode 2 (EN 1992-1-1, 2004), a doubly-reinforced 0.6 m x 0.6 m square pile with a length ($L$) of 6 m and a reinforcement ratio of 2.1% is required. The model diameter of the longitudinal bars and shear links used in this case was 1.25 and 0.6 mm, respectively. The preparation procedures were otherwise identical to those of pile type 1, and utilized the same materials for the model concrete (i.e. 6% copper) and steel wire.

In order to supply different temperatures continually to the model energy piles during testing, the silicon pipes embedded in each model pile were connected to a heating/cooling system (Julabo Ltd; Model F12-ED). The system has a water bath, where any temperature between 1 and 99 °C can be controlled. The system also has a pump, which is able to produce a water flow rate up to 13.5 ml/s. This is sufficient to generate a turbulent flow regime within the embedded pipeline, hence maximizing the convective heat transfer mechanism from the pipes to the model concrete (Loveridge and Powrie, 2013).

**Thermomechanical behavior of model energy pile**

***Free thermal expansion***

The first series of tests were free thermal expansion tests, aiming to determine the CTE of the model pile type 1. Three pairs of strain gages (steel-foil; model no.: SGD-3/120-LY11; Omega Engineering Ltd.) and thermocouples were attached to the pile surface at 105, 170 and 235 mm along the pile length for measuring axial strain mobilization and pile surface temperature, respectively. To minimize temperature effects, half-bridge connections were applied to each pair of strain gages (National Instruments, 2016). One gauge was mounted along the principal axis of strain (i.e., axial direction), while the other one was mounted perpendicularly to this. A layer of epoxy resin with a thickness of about 1 mm was applied on the surface of each strain gage for protection. The epoxy-sand interface has a friction coefficient of 0.53 (Ramadan et al., 2013), which is well within the range for the concrete-sand interface reported by Di Donna et al. (2015) (0.49 – 0.58). In fact, along the 300 mm-long model pile, the three stain gages occupy a length of only 3 mm. Effects of the presence of external strain gages on soil-pile interface are thus

negligible. Each model pile was supported by two stainless steel rollers, so the pile was allowed to expand and contract freely upon heating–cooling cycles. Four heating-cooling cycles were introduced to the model pile by varying the temperature of water between ambient (~22 $^{o}$C) and 50 $^{o}$C (i.e., heating phase). Each pile was heated up until the average pile surface temperature reached a thermal equilibrium, and it was then cooled to the ambient temperature. Each cycle took 40 – 50 min. Inlet and outlet temperature ($T_{in}$ and $T_{out}$) were measured by thermocouples. These measurements were made at the silicon pipes where they enter the top of the model pile. Subsequently, another four cooling-heating cycles (i.e., cooling phase) were applied to the same model piles but varying the temperature of water between ambient (~22 $^{o}$C) and 5 $^{o}$C. During testing, the ambient temperature also varied and this could introduce additional thermal expansion and contraction within the strain gauges. To compensate for this effect, a control experiment was conducted in parallel, consisting of an identical strain gauged-model pile placed next to the tested energy pile, but which was not subjected to heating-cooling cycles. Any thermal strain obtained from this control pile was subtracted from the values obtained from the tested pile.

As can be seen in Fig. 2(a), during all four heating cycles, the loop inlet water temperature ($T_{in}$) was consistently higher than the outlet's ($T_{out}$) by approximately the same temperature difference of 3 $^{o}$C. The temperature difference between $T_{in}$ and $T_{out}$ was likely because a portion of the heat energy of the water that was circulating within the model pile was transferred to the model concrete and model reinforcement due to the temperature gradient between the pipes and the surrounding materials. During the cooling cycles (Fig. 2(b)), there was little difference between $T_{in}$ and $T_{out}$ under the smaller temperature difference ($\Delta T$ = -17 $^{o}$C), compared to the

heating cycles ($\Delta T$ = +28 °C). The pile surface temperature during all heating and cooling cycles was respectively lower and higher than the water temperature due to thermal resistances of the different components of the mortar. Considering that the heat flow in the system obeys Fourier's law, the pile surface temperature ($T_p$) can be estimated by:

$$T_p = T_f + q \sum_i R_i \quad (1)$$

where $T_f$ is the water temperature, which is the mean of $T_{in}$ and $T_{out}$ (Loveridge and Powrie, 2013); $R_i$ is the thermal resistance of component $i$, which in this case includes the silicone pipes, copper powder, sand and plaster; and $q$ is the heat transferred per unit length:

$$q = \frac{m S_c (T_{out} - T_{in})}{L_p} \quad (2)$$

where $m$ is the applied mass flow rate of water (1.6 x $10^{-3}$ kg/s); $S_c$ is the specific heat of water (4187 J/kg K) and $L_p$ is the pipe length (600 mm). To capture the effects of (i) pipe-mortar thermal resistance and (ii) pipe-to-pipe heat exchange within the model pile when estimating $R_i$, the calculation method proposed by Marcotte and Pasquier (2008) is adopted, whereby a shape factor of 11 was applied to take the U-loop pipe arrangement into account. Hence, the equivalent thermal resistance of the model RC pile is 0.25 mK/W (prototype), which is close to the typical range from 0.05 to 0.23 mK/W reported in the literature (Bourne-Webb et al., 2009; Mimouni and Laloui, 2015). By Eq. (1), time histories of calculated $T_p$ are superimposed in Fig. 2. Close agreement is found with the measurements. This verifies the mechanism of heat conduction within the model pile, similar to that normally seen in full-scale RC cases.

Fig. 3 relates the thermally-induced axial strain of pile type 1 with the pile surface temperature change. A recent field study reported by Faizal et al. (2018) shows that the temperature distribution over the cross-section of a full-scale 0.6 m-diameter bored pile was

almost uniform. It is thus a reasonable assumption that the temperature measured at the pile surface at each elevation, and hence thermal strain, was the same as that along the cross-section. At any pile depth, a linear and reversible response is observed. This suggests that for the temperature range examined, the model RC energy pile made of the thermally-enhanced mortar behaved thermally elastically. By estimating the gradient of the linear curves, the CTE of the model pile is 8.9 ± 1.4 με/°C, which is within the range of the linear thermal expansion of concrete (8.5 – 10 με/˚C; Bourne-Webb et al., 2009; Pasten and Santamarina, 2014).

***Compression tests***

The second series of tests conducted were uniaxial compression tests for model pile type 1. The toe of each free-standing model pile was clamped and structurally fixed at a platform. A full moment fixity was thus achieved. The pile head was subjected to a vertical compression using an Instron 5985 load frame under a loading rate of 0.05 MPa/s. To investigate any effect of temperature on the pile axial behavior, three levels of temperature were examined, ambient (19 °C), heating and cooling. For the heating test, the model pile was heated continuously by maintaining the $T_{in}$ at 51 °C. When a thermal equilibrium was reached, an axial load test was conducted (while $T_{in}$ was maintained). The axial behaviour of the model pile was also tested after subjecting to continuous cooling by maintaining the $T_{in}$ at 9 °C. Three test replications were conducted for each temperature level.

Fig. 4 shows typical pile load-displacement curves during the compression at different temperatures. Regardless of the pile temperature applied, the axial load increased almost linearly and reached a distinct peak value between 3 – 3.6 MN (prototype) at an axial strain of around 0.005. Note that in foundation designs, the ultimate structural capacity of pile would

rarely be reached, since the soil underneath would have normally been failed under a lower load. After mobilization of the peak strength, there was a significant reduction of stress. For the application of a piled building foundation, the compressive resistance ($N_{max}$) and axial rigidity ($EA$, where $E$ is Young's modulus and $A$ is gross cross-section area of the model pile) are of most interest. One-way ANOVA was carried out to determine any statistical difference at 5% significance level of the pile axial behavior at the three temperature levels considered. The compressive strength has no statistically-significant difference between 9 and 19 $^{o}$C cases ($p$-value = 0.227 > 0.05). This means that the temperature reduction (from 19 to 9 $^{o}$C; i.e., 10 $^{o}$C difference) was not significant enough to introduce noticeable difference in the pile capacity. However, interestingly, the $p$-value between 19 and 51 $^{o}$C cases is 0.025 < 0.05, meaning that they are statistically different. For $EA$, no significant statistical difference is found for either the pair of 9 and 19 $^{o}$C ($p$-value = 0.136 > 0.05) or 19 and 51 $^{o}$C ($p$-value = 0.588 > 0.05). It is well-known that below 100 $^{o}$C, the mechanical properties of prototype concrete and steel reinforcement, including compressive strength and elastic modulus, are insensitive to temperature change (Takeuchi et al., 1993). For the case of model concrete, some temperature dependency on the compressive strength was found, whereas the $EA$ was much less sensitive. The modelling, however, is deemed satisfactory, because for foundation applications: (i) it is mainly $EA$ that affects pile head settlement and (ii) it is the soil shear strength, not the pile compressive strength, which limits the axial capacity of a soil-pile system.

***Four-point bending (FPB) tests***

The third series of tests was conducted to characterize any effects of temperature on flexural behavior of the model pile type 2 via FPB tests. Water of different temperature (5 $^{o}$C, ambient

(20 $^{o}$C), 35 $^{o}$C and 50 $^{o}$C) was circulated to each model pile until a thermal equilibrium was reached, as indicated by the three thermocouples attached on the pile surface in each test. Each model pile was then loaded to give a constant moment over the central third of the beam to obtain a moment-curvature curve. A test was complete when the pile mid-section exhibited large deformation and formed prominent cracking (at tensile strains of 0.016 – 0.048%). Model piles mixed with 0, 6 and 12% copper powder were examined. Three replicates were tested for each amount of copper powder and each temperature level.

Fig. 5 compares typical moment-curvature relationships of the model piles tested at different temperatures. A curve predicted by an open-source section-analysis software, KSU_RC (Esmaely, 2013), at the ambient temperature of 20 $^{o}$C, is also shown for reference. The nonlinear stress-strain behavior of RC used in KSU_RC was that proposed by Mander et al. (1998) and the behavior of steel reinforcement is linear-elastic-perfectly-plastic. All model piles, regardless of the level of temperature tested, show an abrupt drop of moment near the peak value as major cracks formed. Ductile behavior is observed, as all model piles do not show any sign of ultimate collapse after a large curvature higher than 0.05 $m^{-1}$. Some of the observed differences of responses were associated with experimental uncertainties such as material variabilities and workmanship. Indeed, the model RC exhibited similar coefficient of variation (COV) of bending strength to the full-scale RC (< 10%; Knappett et al. (2018)). As can be seen in the inset of the figure, after tests, prominent bending cracks were recreated, realistically replicating the important quasi-brittle behavior found in prototype RC.

Fig. 6 shows the effects of temperature and copper powder content on peak bending moment and flexural rigidity (*EI*; taken as the initial linear portion of the moment-curvature curve between

30% and 50% of the peak moment). Without copper powder (0%), both moment capacity (Fig. 6(a)) and *EI* (Fig. 6(b)) apparently increase with an increase in pile temperature, but these trends are statistically not significant (*p*-value always > 0.05). For the 6% case, no specific trend can be found between pile temperature and its flexural properties (*p*-value always > 0.05). This is consistent with the fact that the mechanical properties of concrete and steel are less affected when the temperature applied is less than 100 $^{o}$C (Takeuchi et al., 1993). With 12%, copper, however, evident drops of both bending moment and *EI* can be seen. Indeed, *p*-values in both cases are less than 0.05, meaning that the addition of 12% copper powder affected the flexural properties statistically significantly.

Based on the observed properties of the new model concrete and the thermomechanical axial and flexural behavior of the model piles, with support of statistical testing, it appears that an optimum copper powder content that could enhance the thermal properties of the model concrete by Knappett et al. (2011) but without adversely affecting the mechanical response of the model structure is 6%. The theoretical peak bending moment and *EI* predicted by the KSU_RC was 325 kNm and 41 MNm$^2$, respectively. These values are deemed acceptably close to the laboratory-measured average peak moment (336 kNm) and average *EI* (33 MNm$^2$).

**Thermomechanical soil-pile interaction at 1-g**

To illustrate the effectiveness of using the new mode RC to model the axial thermomechanical behavior of energy piles in soil, 1-g physical model tests were performed. These tests are illustrative and they aim to explore whether key thermomechanical pile-soil interaction phenomena could be reproduced qualitatively, ahead of subsequent centrifuge tests (not

reported here). Although relevant scaling laws and non-dimensional groups (see below) are utilized to ensure similitude in behavior, there is no intention to quantitatively compare prototype responses with field observations in this simple 1-g experiment.

***Scaling laws and similitudes***

Considering that the sand used in the 1-g tests has the same density as that of the prototype and the shear modulus ($G$) of such a soil is proportional to the square root of effective confining pressure, the so-called 'Type II' scaling laws proposed by Iai et al. (2005) may be used. The scaling laws for soil and pile properties are summarized in Table 1.

In order to achieve similitude, the relative soil-pile stiffness and strength must be scaled appropriately. Non-dimensional relative axial stiffness can be described by the ratio of the elastic stiffness of the soil to the axial pile structural stiffness (Randolph and Wroth, 1978):

$$\left(\frac{L^2 G}{EA}\right)_m = \left(\frac{L^2 G}{EA}\right)_p \tag{3}$$

where the subscript $m$ and $p$ refers to the model and prototype scale, respectively. This similitude is satisfied using both the 1-g and high-g scaling laws from Table 2. Non-dimensional relative axial strength can be described by the ratio of the structural pile strength ($Q_{pile}$) to the bearing capacity of the pile (proportional to (i) $N_q \sigma'_v A$ at the pile base, where $N_q$ is bearing capacity coefficient which is a function of friction angle ($\phi$); $\sigma'_v$ is vertical effective stress; $A$ is pile sectional area, and to (ii) $\beta \sigma'_v BL$ along the shaft, where $\beta = Ktan\delta$; $K$ is earth pressure coefficient; $\delta$ is soil-pile interface friction angle; $B$ is pile circumference):

$$\left(\frac{Q_{pile}}{N_q(\phi)\sigma'_v A}\right)_m = \left(\frac{Q_{pile}}{N_q(\phi)\sigma'_v A}\right)_p \tag{4a}$$

$$\left(\frac{Q_{pile}}{4\beta(\phi)\sigma'_v L}\right)_m = \left(\frac{Q_{pile}}{\beta(\phi)\sigma'_v BL}\right)_p \tag{4b}$$

These relationships are satisfied if the friction angle is the same in the model and prototype. This is ensured in the centrifuge (high-g) as the effective stress levels are representative of prototype conditions. At 1-g, the operative friction angle would be higher in the model than the prototype due to increased dilation at low confining effective stress. This would suggest that structural failure would be biased in the model; however, in the tests presented here, the capacity was observed to be controlled by soil failure.

To scale the heat flow in soil, the non-dimensional number, Fourier's number (which is derived from the 2nd law of heat diffusion), may be used:

$$\left(\frac{at}{L^2}\right)_m = \left(\frac{at}{L^2}\right)_p \quad (5)$$

where $a$ is soil thermal diffusivity; and $t$ is heat diffusion time. Since (i) the same sand was considered in the model and prototype scale (i.e., scaling factor of $a$ is 1) and (ii) the scaling factor of $L$ is $N$ (Table 2), for similitude, the scaling factor for $t$ must be scaled by $N^2$.

According to Table 1, mechanical strain is scaled by $N^{0.5}$. To consider thermomechanical coupling, the scale factor for mechanical strain has to be the same as that for thermal strain ($\varepsilon_T$), so it should also be scaled by $N^{0.5}$. Considering thermal elasticity,

$$\varepsilon_T = \alpha_T \Delta T \quad (6)$$

where $\alpha_T$ is coefficient of thermal expansion; and $\Delta T$ is temperature change. Again, since (i) $\varepsilon_T$ is non-dimensional; (ii) the same sand is considered in the model and prototype scale (i.e., scaling factor of $\alpha_T$ is 1); and (iii) $\varepsilon_T$ is scaled by $N^{0.5}$, $\Delta T$ must be scaled by $N^{0.5}$.

***Test setup and procedures***

In this test, a 1:35 scale model energy pile type 1 (6% copper powder) was installed "wish-in-placed" in the center of a uniform bed of HST 95 Congleton silica sand in a model container (Fig.

7). As the model pile was suspended in position, the sand was air pluviated surrounding the pile to produce a uniform sand deposit with a height of 350 mm at an average relative density $D_r$ of 74%. The mechanical properties of the sand at this specific $D_r$ are summarized in Table 2. The model pile was instrumented with a vertical array of three thermocouples and strain gages for measuring pile surface temperature and any thermally-induced pile axial strain at 5, 70 and 135 mm depth. The pile embedment depth was 200 mm, leaving the top 100 mm above the soil surface. The model box was hydraulically insulated, but not thermally. The model pile was installed at 11 times diameter (D; i.e., 11D) away from the side boundary and 8D away from the bottom. Based on the limited field data available in the literature (e.g., Mimouni and Laloui, 2015), the radial influence zone of soil temperature induced by pile heating and cooling is typically ~ 4D. Hence, the pile heating and cooling processes introduced by the model pile in this study are not expected to be subjected to any thermal boundary effect. The distance between the pile toe and the bottom of the sand bed ($8D$) was sufficient to avoid boundary effects on the pile base capacity (Knappett et al., 2016). From this point onwards, all dimensions are expressed in prototype scale.

The test consisted of four phases, representing different proportions of the pile capacity (i.e. working loads for different factors of safety). In each phase, (i) the maintained vertical working load was initially applied using the Instron 5985 load-frame under load-control at a rate of 0.05 MPa/s, followed by (ii) four heating–cooling cycles and (iii) mechanical unloading to zero head load. Time histories of the mechanical and thermal loads applied are shown in Fig. 8. The working loads applied in the first, second, third and fourth phases represented 0, 13, 51 and 89% of the ultimate pile capacity (1741 kN; much less than the ultimate structural capacity in Fig. 4),

respectively. The ultimate capacity was determined by the sum of the shaft and base resistances, following the Terzaghi's bearing capacity equation and the calculation procedures outlined in Eurocode 7 (EN 1997-1, 2004). For the cohesionless sand having a friction angle of 32$^{o}$, the bearing capacity factors associated with overburden pressure ($N_q$) and cohesion ($N_c$) is 23 and 0 (Knappett and Craig, 2012), respectively. During thermal cycling, water with $T_{in}$ varying between 12 and 45 $^{o}$C (ambient temperature of 22 $^{o}$C) was circulated within the model piles (Fig. 8(b)). Identical heating–cooling cycles were applied in all four phases. Pile head displacement, pile surface temperature, pile axial load mobilization and soil temperature were monitored continuously throughout the test.

***Test results***

Fig. 9 shows the thermally-induced pile head displacement. In general, the pile head heaved upon heating and settled upon cooling, as expected. When the pile head was not constrained (i.e., 0% working load), the pile head displacement was almost fully reversible. When the pile head was more mechanically constrained (i.e. higher applied working load), irreversible ratchetting pile head settlement was increasingly significant. The same behavior was identified qualitatively in both laboratory 1-g test (Yavari et al., 2014) and centrifuge testing (Ng et al., 2015) using aluminum alloy pile models and from numerical simulations (Pasten and Santamarina. 2014; Zhao et al., 2017). The model pile, with the use of the new model concrete, can reproduce the soil-structure interaction behavior of RC energy piles.

Time history of thermomechanical strains during all four phases are presented in Fig. 8(c). Based on the coefficient of thermal expansion of the model pile determined from the free thermal expansion tests (refer to Fig. 3) and the known time history of temperature in this tests,

theoretical free thermal strain was determined. The corresponding time history is superimposed in Fig. 8(c) for reference. As expected, the amplitude of strain fluctuation at all three depths in any loading stage cycle was less than that of the free thermal strain due to the constraint of the surrounding soil where soil-pile interface friction exists. This explains why for a given applied working load, the strain mobilized near the ground surface was greater than at depth. Apparently, under any working load, the pile strains mobilized at all depths were almost reversible during the four heating/cooling cycles. This seems to imply that the soil-pile interaction may be largely thermo-elastic. Indeed, upon heating or cooling of silica sand, only very limited thermo-plastic response has previously been observed (Ng et al., 2015). It has been recently advocated that thermo-elasticity may be sufficient to capture the behavior of RC energy piles installed in sand (Rotta Loria and Laloui, 2016; Zhao et al., 2017). The strain results suggest that the plastic pile head settlement observed under high working load in Fig. 9 was associated with the continual plastic straining of the soil beneath the pile toe, as consistently found in the numerical prediction made by Zhao et al. (2017).

**Summary and conclusions**

This study presents a new type of model concrete that is suitable for realistically modelling the thermo-mechanical behavior of energy piles and their interaction with the surrounding soil. The new model concrete is a thermally-enhanced mortar. It is a mixture of plaster, water and sand to geometrically scale the aggregate and copper powder to improve the thermal properties of the mixture. It was revealed that 6% of copper powder (by volume) is an optimal value for the new model concrete, matching the coefficient of thermal expansion and thermal conductivity of field

concrete, while not detrimentally affecting the mechanical properties.

The model concrete was used to construct two small-scale RC energy piles of different dimensions and scales to examine their axial and lateral thermomechanical behavior in soils. Besides model reinforcement, silicon pipes arranged in U-shaped loops were embedded in each pile for allowing water of different temperatures to be circulated through the pile. Controlled pile heating/cooling could hence be applied to the surrounding soil, allowing pipe-concrete-soil heat transfer efficiency to be evaluated. This is a unique feature of the new model concrete that most existing small-scale piles modelled by, for example, aluminum alloy, cannot achieve. Given the range of pile temperature tested (5 – 50 $^{o}$C) and 6% of copper powder content added, key axial and flexural stiffness of the model RC piles were not temperature sensitive, which is consistent with field RC.

As revealed from the 1-g tests, temperature-induced cyclic pile head settlement (ratchetting) for piles under vertical maintained load, as typically observed in field energy pile systems for buildings, was reproduced in the laboratory when the new type of model RC pile was heated and cooled consecutively in a uniform soil deposit. Consistent with the findings of most of the field testing and finite-element modelling reported in the literature, the pile head ratcheting measured increased with an increase in the working load applied on the pile head. The range of thermally-induced pile axial strain is reasonably close to existing field data.

**Acknowledgments**

The first author (RZ) acknowledges the studentship provided by the Chinese Scholarship Council. The second (AL) and third (DV) authors thank the research expenditures provided by Energy

Technology Partnership (ETP), Scottish Road Research Board (SRRB) from Transport Scotland, the EPSRC Doctoral Training Award as well as the Scottish Funding Council (SFC).

**References**

Al-Defae, A. H., and Knappett, J. A. (2014). "Centrifuge modeling of the seismic performance of pile-reinforced slopes." *J. Geotech. Geoenviron. Eng., ASCE*, 140(6), p.04014014.

Bažant, Z. P. (2005). *Scaling of structural strength*. Elsevier Butterworth-Heinemann, UK.

Belgin, C. M. and Sener, S. (2008). "Size effect on failure of over reinforced concrete beams." *Eng. Fract. Mech.,* 75, 2308–2319.

Bourne-Webb, P. J., Amatya, B., Soga, K., Amis, T., Davidson, C. and Payne, P. (2009). "Energy pile test at Lambeth College, London: geotechnical and thermodynamic aspects of pile response to heat cycles." *Géotechnique*, 59(3), 237-248.

Brandl, H. (2006). "Energy foundations and other thermo-active ground structures." *Géotechnique*, 56(2), 81-122.

Broms, B. (1964). "Lateral Resistance of Piles in Cohesionless Soils". *J. Soil Mech. Found. Div.,* 90(3), 123-158.

Chen, D. and McCartney, J.S. (2017). "Parameters for load transfer analysis of energy piles in uniform nonplastic soils." *Int. J. of Geomech*., *ASCE*, 17(7), 04016159.

Di Donna, A., Ferrari, A. and Laloui, L., (2015). "Experimental investigations of the soil–concrete interface: physical mechanisms, cyclic mobilization, and behaviour at different temperatures". *Can. Geotech. J.,* 53(4), 659-672.

El Zeiny, R., Suleiman, M. T., Abu Qamar, M., Xiao, S., and Al-Khawaja, M. (2018). "Axial Pull-out

Response of a Small Scale Concrete Pile Subjected to Cyclic Thermal Loading in Sand." *Int. Found. Cong. Equip. Expo 2018*, 709-714.

Esmaely, A. (2013). "KSU_RC: Moment Curvature, Force Deflection and Interaction Analysis of RC Members". Civil Engineering Department, Kansas State University.

Faizal, M., Bouazza, A., McCartney, J. S., and Haberfield, C. (2018). "Axial and radial thermal responses of an energy pile under a 6-storey residential building". *Can. Geotech. J.,*(999), 1-15.

Goode, J., III, and McCartney, J. S. (2015). "Centrifuge modeling of boundary restraint effects in energy foundations." *J. Geotech. Geoenviron. Eng., ASCE*, 141(8), p.04015034.

Ground Source Heat Pump Association (GSHP). (2012). *Thermal pile design, installation and materials standards,* Milton Keynes, UK.

Hayward, T., Lees, A., Powrie, W., Richards, D. J., and Smethurst, J. (2000). "Centrifuge modelling of a cutting slope stabilised by discrete piles." *Rep. 471, Transport Research Laboratory*, Berkshire, UK.

Iai, S., Tobita, T. and Nakahara, T., (2005). "Generalised scaling relations for dynamic centrifuge tests". *Géotechnique,* 55(5), 355-362.

Jeong, S., Kim, B., Won, J., and Lee, J. (2003). "Uncoupled analysis of stabilizing piles in weathered slopes". *Comput. Geotech.*, 30(8), 671-682.

Knappett, J. A., and Craig, R. F. (2012). *Craig's soil mechanics,* 8th Ed., London, UK: Spon Press.

Knappett, J. A., Reid, C., Kinmond S., and O'Reilly, K. (2011). "Small-Scale Modeling of Reinforced Concrete Structural Elements for Use in a Geotechnical Centrifuge". *J. Struct. Eng., ASCE*, 137(11), 1263-1271.

Knappett, J. A., Caucis, K., and Brown, M. J. (2016). “CHD pile performance: Part II – numerical modelling”. *Proc. Inst. Civ. Eng. Geotech. Eng.,* 169(5), 436-454.

Knappett, J. A., Brown, M. J., Shields, L., Al-Defae, A. H. and Loli, M. (2018). “Variability of small scale model reinforced concrete and implications for geotechnical centrifuge testing”. *Proc. 9th Int. Conf. on Physical Modelling in Geotechnics* (ICPMG 2018), CRC Press, Taylor & Francis Group, London, U. K., 241-246.

Loli, M., Knappett, J. A., Brown, M. J., Anastasopoulos, I., and Gazetas, G. (2014). “Centrifuge modeling of rocking-isolated inelastic RC bridge piers.” *Earthquake Eng. Struct. Dyn.,* 43(15), 2341-2359.

Loveridge, F. and Powrie, W. (2013). “Pile heat exchangers: thermal behaviour and interactions.” *Proc. Inst. Civ. Eng. Geotech. Eng.,* 166(2), 178-196.

Mander, J., Priestley, M. J. N., and Park, R. (1988). "Theoretical stress-strain model for confined concrete." *J. Struct. Eng., ASCE*, 114(8), 1804-1826.

Marcotte, D. and Pasquier, P. (2008). "On the estimation of thermal resistance in borehole thermal conductivity test." *Renewable Energy*, 33(11), 2407-2415.

McCartney, J. S. and Rosenberg, J. E., (2011). “Impact of heat exchange on side shear in thermo-active foundations”. *In Geo-Frontiers 2011: Advances in Geotechnical Engineering*, 488-498.

Mimouni, T. and Laloui, L. (2015). “Behaviour of a group of energy piles”. *Can. Geotech. J.,* 52(12), 1913-1929.

Murphy, K. D. and McCartney, J. S. (2015). “Seasonal response of energy foundations during building operation”. *Geotech. Geol. Eng.,* 33(2), 343-356.

National Instruments. (2016). “Measuring strain with strain gauge”. < http://www.ni.com/white-

paper/3642/en/> (May. 25, 2016).

Ng, C. W. W, Shi, C., Gunawan, A., Laloui, L., Liu, H. L. (2015). "Centrifuge modelling of heating effects on energy pile performance in saturated sand." *Can. Geotech. J.,* 52(8), 1-13.

Pasten, C. and Santamarina, C. (2014). "Thermally induced long-term displacement of thermoactive piles*". J. Geotech. Geoenviron.Engng, ASCE*, 140(5), p.06014003.

Ramadan, M.I., Butt, S.D., and Popescu, R. (2013). "Offshore anchor piles under mooring forces: numerical modeling". *Can. Geotech. J.,* 50(2), 189–199.

Randolph, M.F. and Wroth, C.P. (1978). "Analysis of deformation of vertically loaded piles". *J. of the Geotech. Eng. Div.*, *ASCE,* 104(GT12), 1465–1488.

Rotta Loria, A. F. and Laloui, L. (2016). "Thermally induced group effects among energy piles." *Géotechnique,* 67(5), 374-393.

Rotta Loria, A. F., Di Donna, A. and Laloui, L. (2015). "Numerical study on the suitability of centrifuge testing for capturing the thermal-induced mechanical behavior of energy piles." *J. Geotech. Geoenviron. Eng*, *ASCE*, 141(10), 04015042.

Stewart, M. A. and McCartney, J. S. (2014). "Centrifuge modeling of soil-structure interaction in energy foundations." *J. Geotech. Geoenviron. Eng*, *ASCE*, 140(4), p.04013044.

Takeuchi, M., Hiramoto, M., Kumagai, N., Yamazaki, N., Kodaira, A., and Sugiyama, K. (1993). "Material properties of concrete and steel bars at elevated temperatures". *Transactions, 12$^{th}$ SMiRT Int. Conf.,* V.H, *Stuttgart,* 133-138.

Xiao, S., Suleiman, M. T., Elzeiny, R., Naito, C., Neti, S., and Al-Khawaja, M. (2018). "Effect of Temperature and Radial Displacement Cycles on Soil-concrete Interface Properties Using Modified Thermal Borehole Shear Test." *J. of Geotech. Geoenviron. Eng, ASCE*, 144(7),

p.04018036.

Yavari, N., Tang, A. M., Pereira, J. M. and Hassen, G. (2014). “Experimental study on the mechanical behaviour of a heat exchanger pile using physical modelling”. *Acta Geotech.*, *9*(3), 385-398.

Zhao, R., Leung, A. K. and Anastasopoulos, I. (2017). “Numerical investigation of the capacity and settlement of a thermo-active pile in saturated sand”. *In Proc. of the 70th Can. Geotech. Conf. and the 12th Joint CGS/IAH-CNC Groundwater Conf.,* The Canadian Geotechnical Society, Canada.

**List of table captions**

**Table 1.** A summary of relevant scaling factors (i.e., N = prototype/model) for thermomechanical soil-structure interaction problems in 1-g and high-g (after Iai et al. 2005)
**Table 2.** Properties of soil used in the physical model tests

**List of figure captions**
**Figure 1**. Cross-section and reinforcement layouts of the model RC energy piles at type 1 and type 2 (all dimensions expressed at model scale).
**Figure 2**. Time histories of water temperature (inlet and outlet) and pile surface temperature: (a) during four heating cycles and (b) during four cooling cycles, for the free thermal expansion tests.
**Figure 3**. Relation between thermally-induced axial strain and pile surface temperature change.
**Figure 4**. Typical axial force-displacement curves obtained from free-compression tests of model pile type 1 at three different temperatures, all expressed in prototype scale following $N$ = 35 and using the high-g scaling factors in Table 1.
**Figure 5**. Typical moment-curvature curves obtained from four-point bending tests of model pile type 2 at three different temperatures, all expressed in prototype scale following $N$ = 24 and using the high-g scaling factors in Table 1.
**Figure 6**. Temperature effects on (a) peak bending moment and (b) flexural rigidity of model pile type 2, all expressed in prototype scale following $N$ = 24 and using the high-g scaling factors in Table 1.
**Figure 7**. Schematic setup for maintained-axial load thermal cyclic tests for model pile type 1 at 1-g. All dimension in mm in model scale.
**Figure 8**. Time histories of (a) applied vertical load, (b) pile surface temperature and (c) thermally-induced axial strain of the model pile types 1 when subjected to cyclic pile thermal loading under maintained working loads (WL), all expressed in prototype scale following $N$ = 35 and using the 1-g scaling factors in Table 1.
**Figure 9**. Pile head displacement when subjected to cyclic pile thermal loading under maintained working loads (WL), all expressed in prototype scale following $N$ = 35 and using the 1-g scaling factors in Table 1.

**Table 1.** A summary of relevant scaling factors (i.e., N = prototype/model) for thermomechanical soil-structure interaction problems in 1-g and high-g (after Iai et al. 2005)

| **Quantity** | **1-g scale factor** | **High-g scale factor** |
|---|---|---|
| *General* | | |
| Length | N | N |
| Density | 1 | 1 |
| Stress | N | 1 |
| Strain (mechanical) | $N^{0.5}$ | 1 |
| Stiffness | $N^{0.5}$ | 1 |
| *Structural properties* | | |
| Bending stiffness, *EI* | $N^{4.5}$ | $N^4$ |
| Axial stiffness, *EA* | $N^{2.5}$ | $N^2$ |
| Axial force | $N^3$ | $N^2$ |
| Axial displacement | $N^{1.5}$ | N |
| Bending moment | $N^4$ | $N^3$ |
| *Temperature-related* | | |
| Strain (thermal) | $N^{0.5}$ | 1 |
| Time (diffusion) | $N^2$ | $N^2$ |
| Temperature change | $N^{0.5}$ | 1 |

**Table 2.** Properties of soil used in the physical model tests

| **Parameters** | **HST95 silica sand** |
|---|---|
| *State-independent* | |
| Physical properties | |
| Specific gravity, $G_s$ | 2.63 |
| Maximum void ratio, $e_{max}$ | 0.769 |
| Minimum void ratio, $e_{min}$ | 0.467 |
| Critical friction angle, $\phi_{cri}$ (°) | 32 |
| Thermal properties | |
| Coefficient of thermal expansion (με/°C) | 0.55 – 0.75 |
| *State-dependent* | |
| Physical properties | |
| Peak friction angle, $\phi_p$ (°) | 44 |
| Dilation angle, $\varphi$ (°) | 14.5 |
| Young's modulus, $E$ (MPa) | 38.7 |
| Unit weight, $\gamma$ (kN/m$^3$) | 16.6 |
| Thermal properties | |
| Thermal conductivity (W/(m K)) | 0.54 |
| Specific heat (J/(kg K)) | 830 |

**Note:** the physical properties of the HST95 silica sand are from Al-Defae et al. (2014).

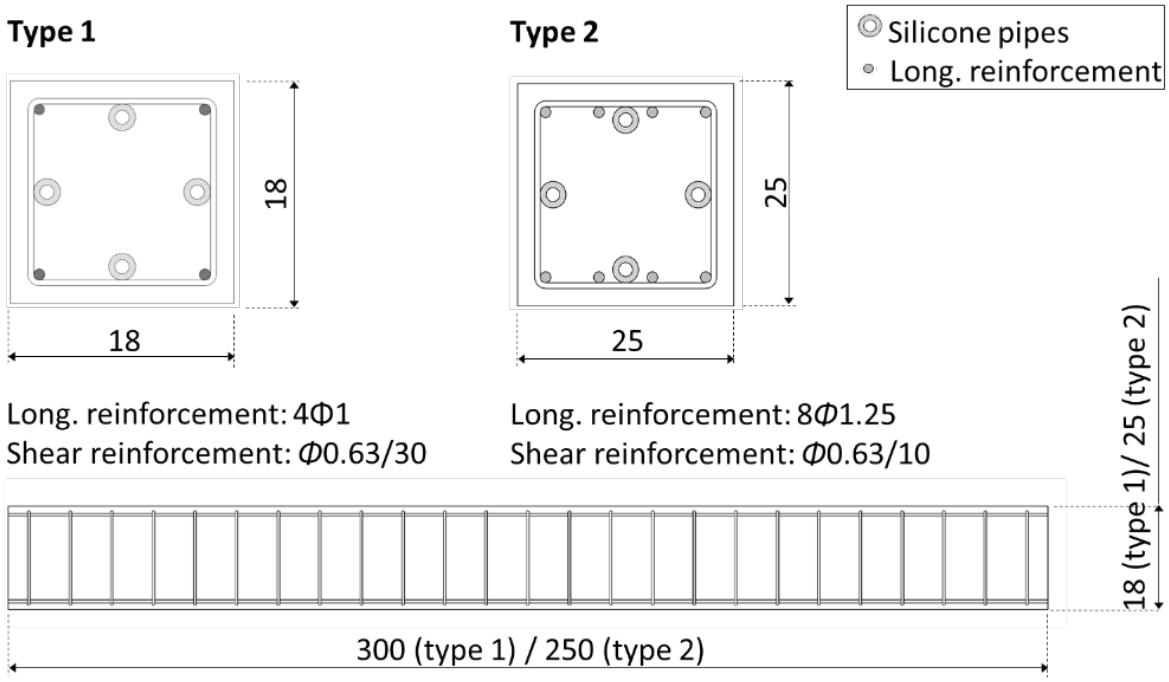


Figure 1. Cross-section and reinforcement layouts of the model RC energy piles at type 1 and type 2 (all dimensions expressed at model scale).

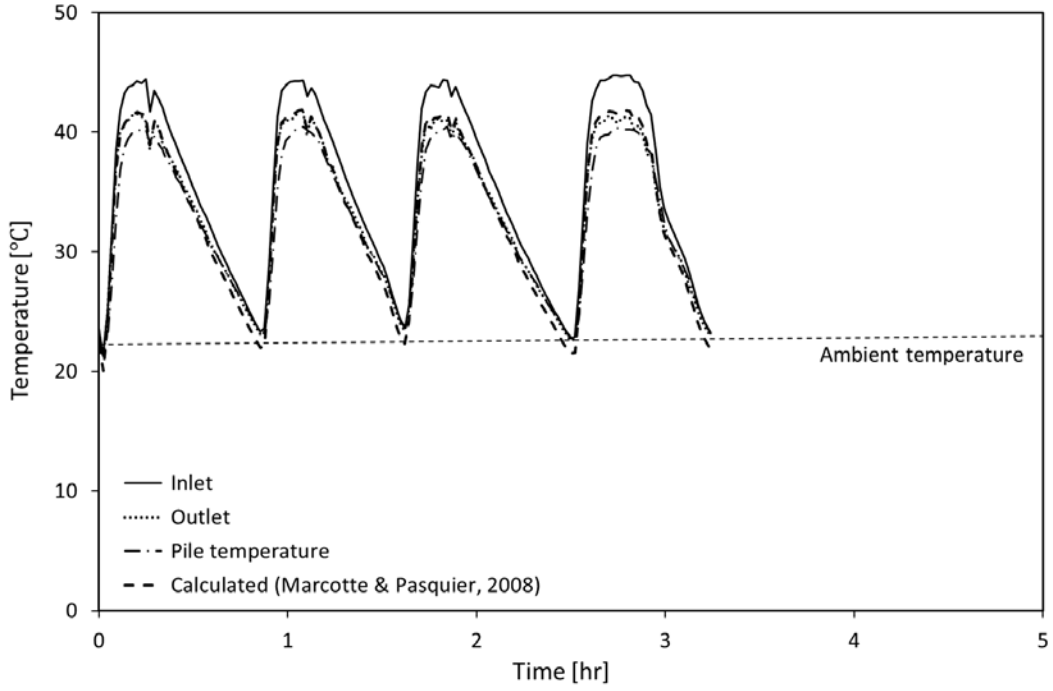


(a)

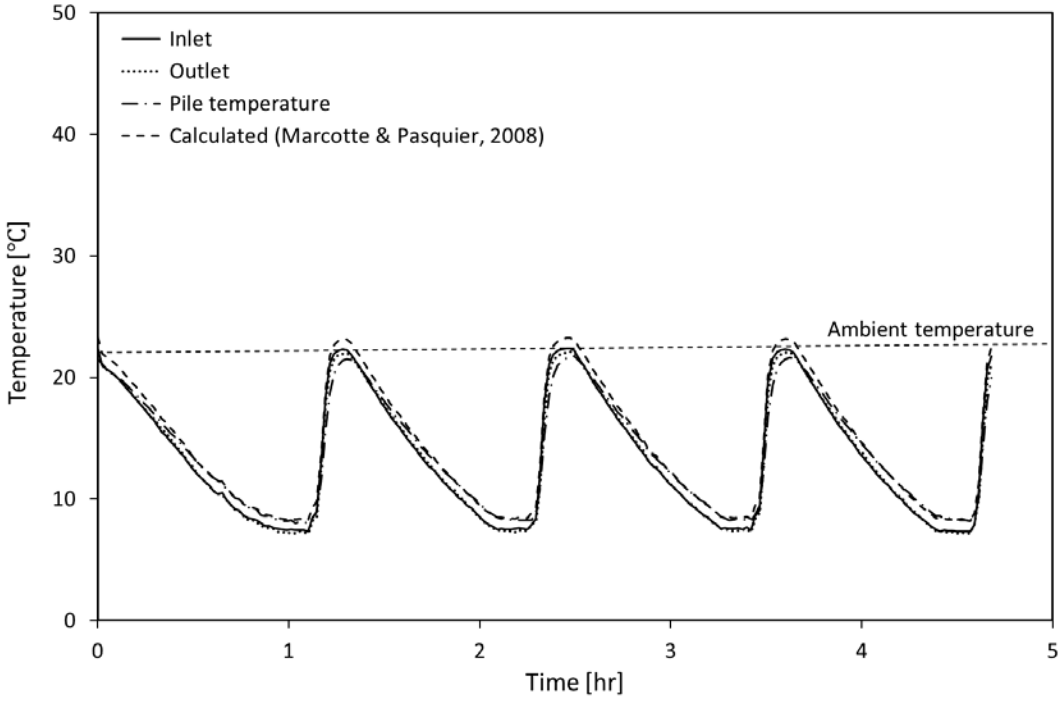


(b)

Figure 2. Time histories of water temperature (inlet and outlet) and pile surface temperature: (a) during four heating cycles and (b) during four cooling cycles, for the free thermal expansion tests.

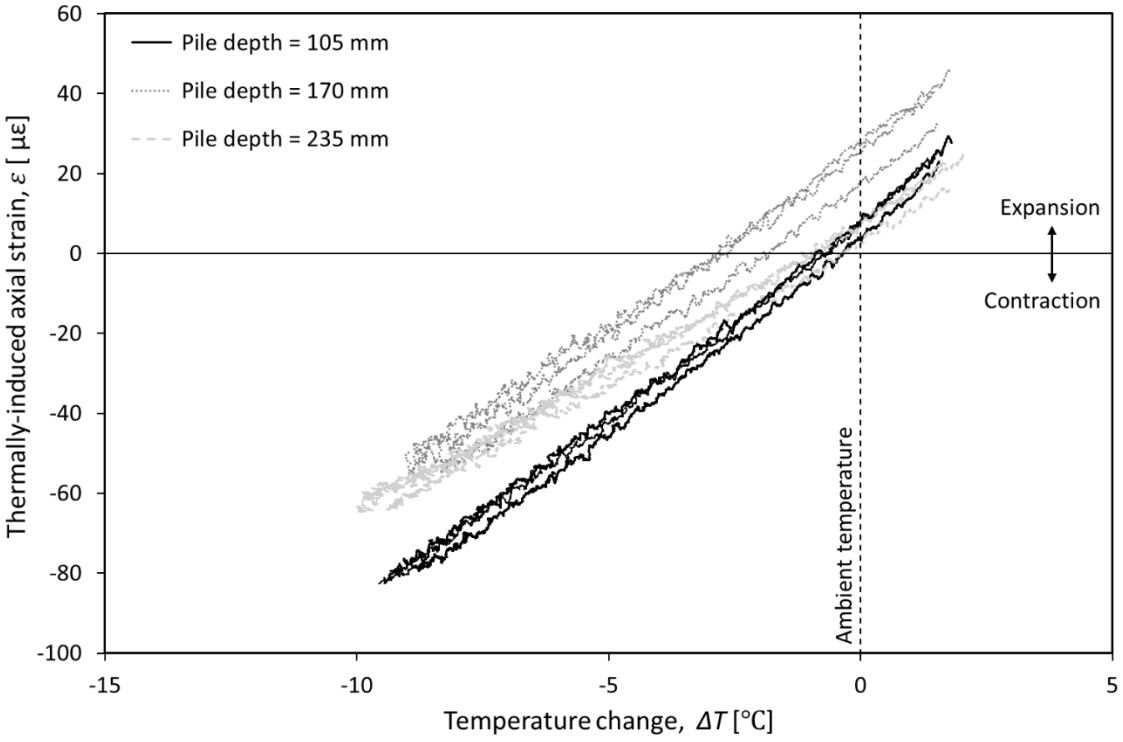


Figure 3. Relation between thermally-induced axial strain and pile surface temperature change.

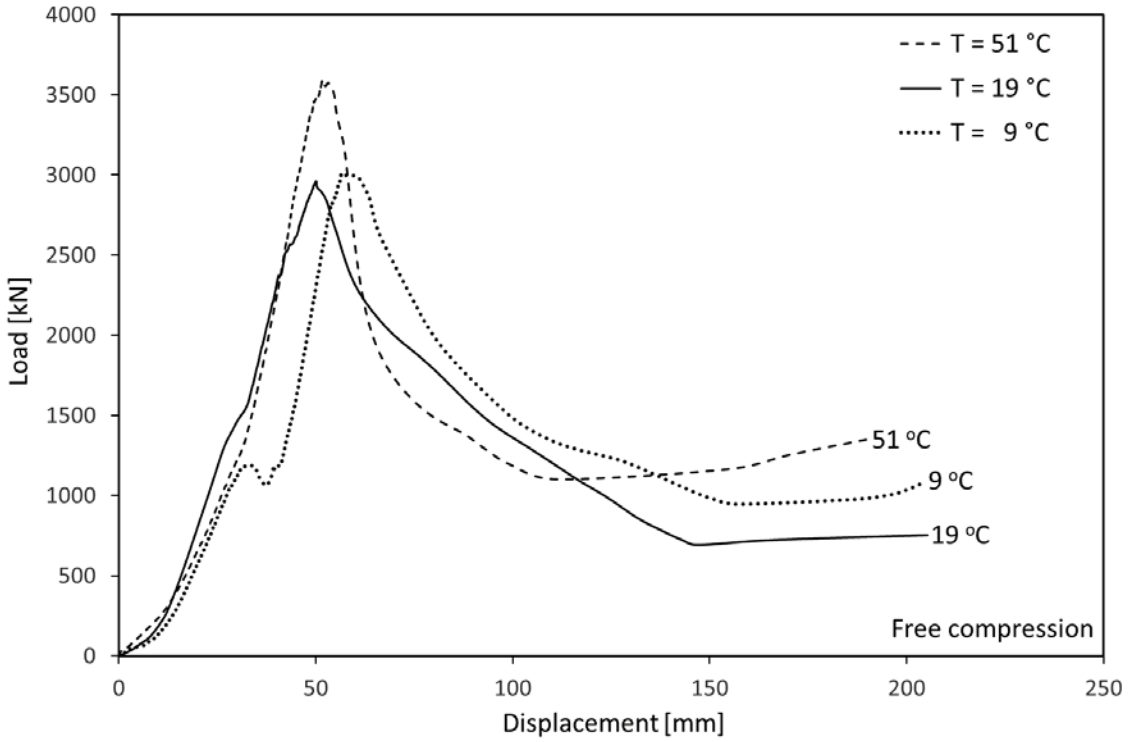


Figure 4. Typical axial force-displacement curves obtained from free-compression tests of model pile type 1 at three different temperatures, all expressed in prototype scale following $N$ = 35 and using the high-g scaling factors in Table 1.

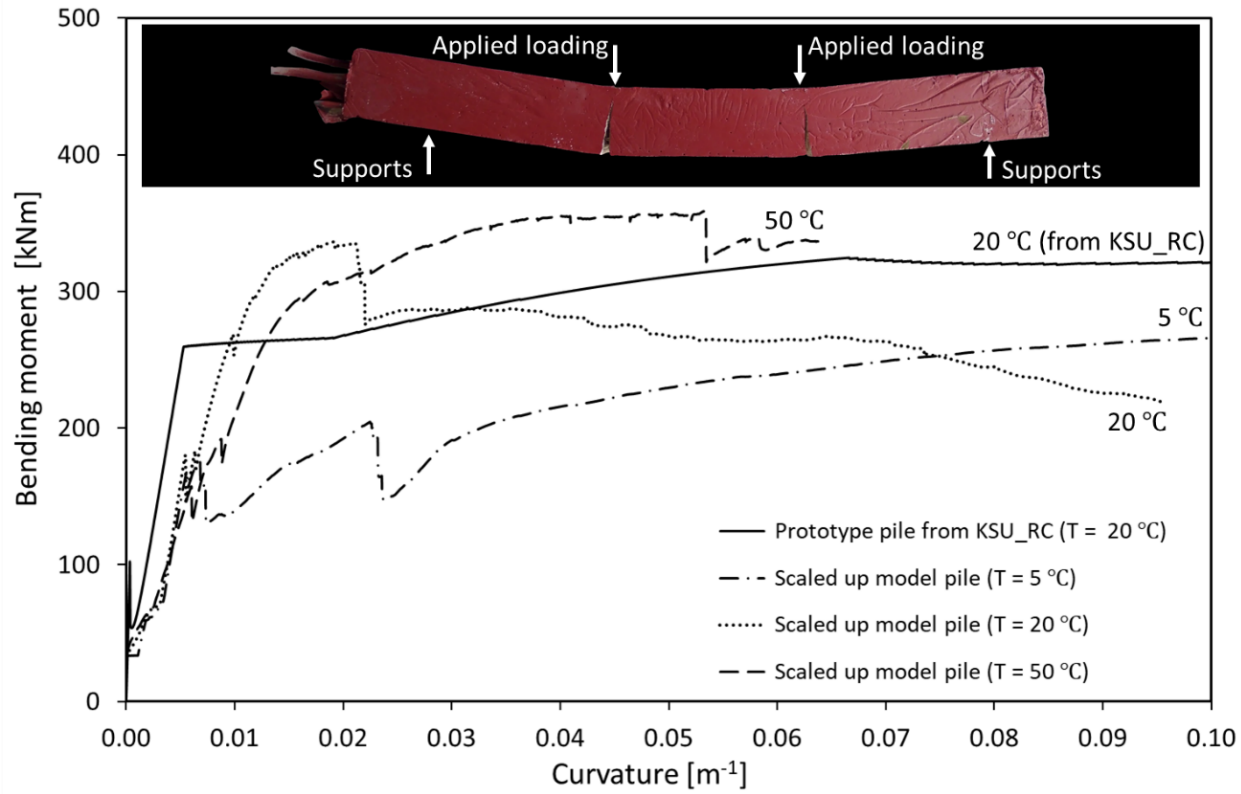


Figure 5. Typical moment-curvature curves obtained from four-point bending tests of model pile type 2 at three different temperatures, all expressed in prototype scale following $N$ = 24 and using the high-g scaling factors in Table 1.

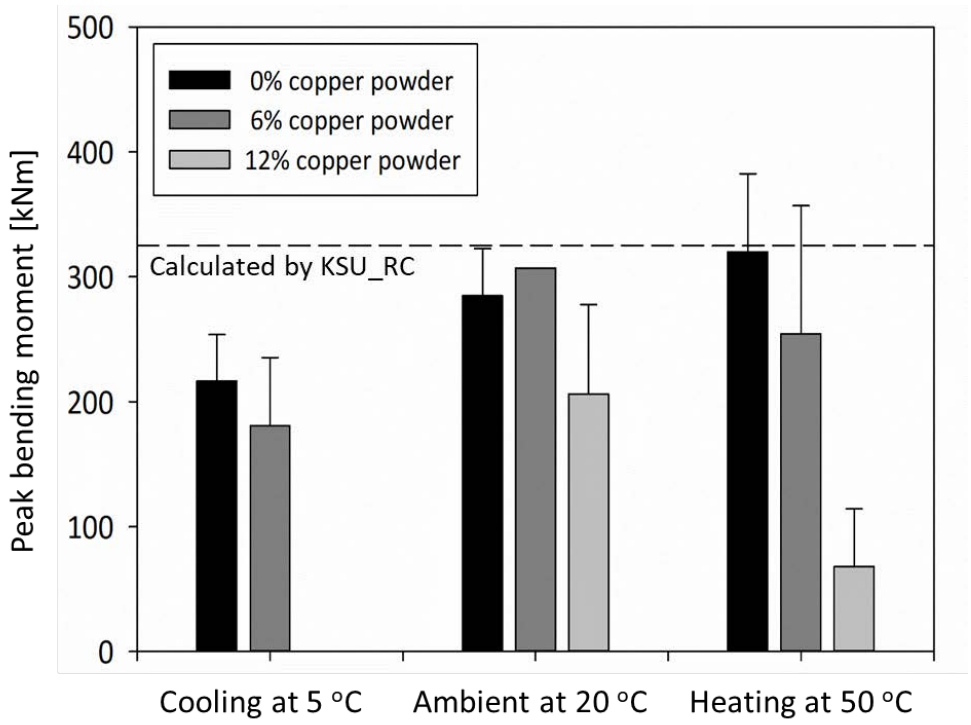


(a)

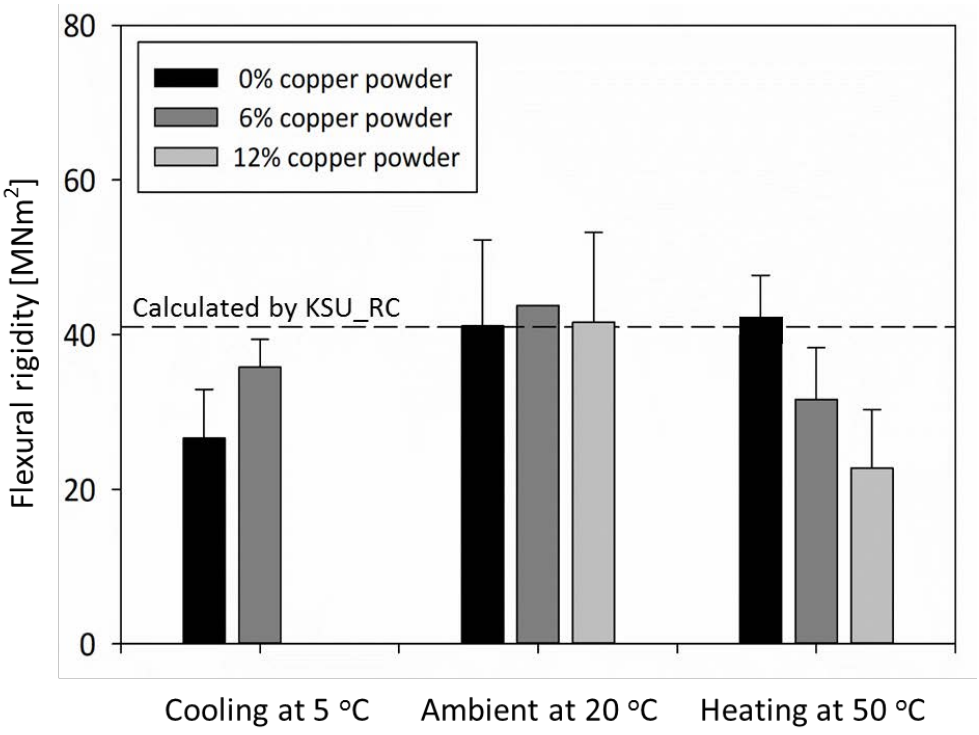


(b)

Figure 6. Temperature effects on (a) peak bending moment and (b) flexural rigidity of model pile type 2, all expressed in prototype scale following $N$ = 24 and using the high-g scaling factors in Table 1.

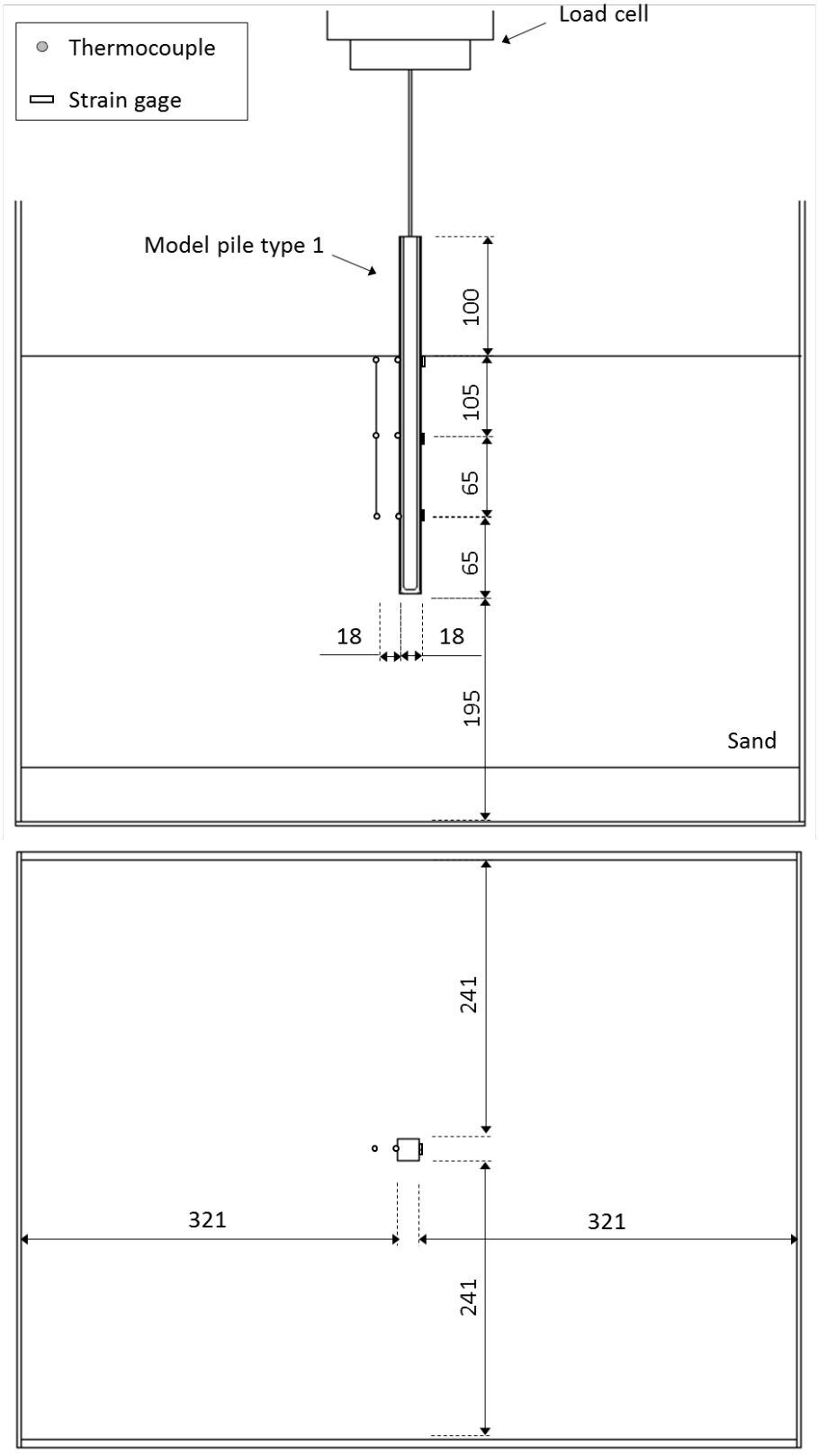


Figure 7. Schematic setup for maintained-axial load thermal cyclic tests for model pile type 1 at 1-g. All dimension in mm in model scale.

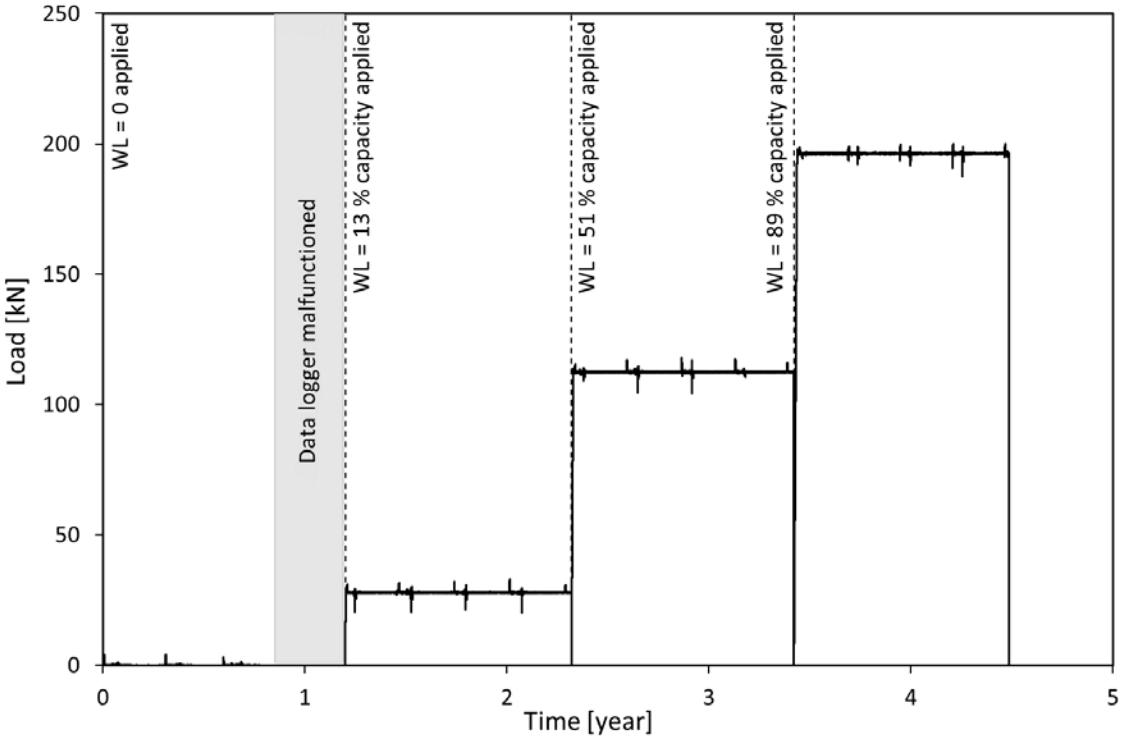
Load [kN]
Time [year]
WL = 0 applied
Data logger malfunctioned
WL = 13 % capacity applied
WL = 51 % capacity applied
WL = 89 % capacity applied

(a)

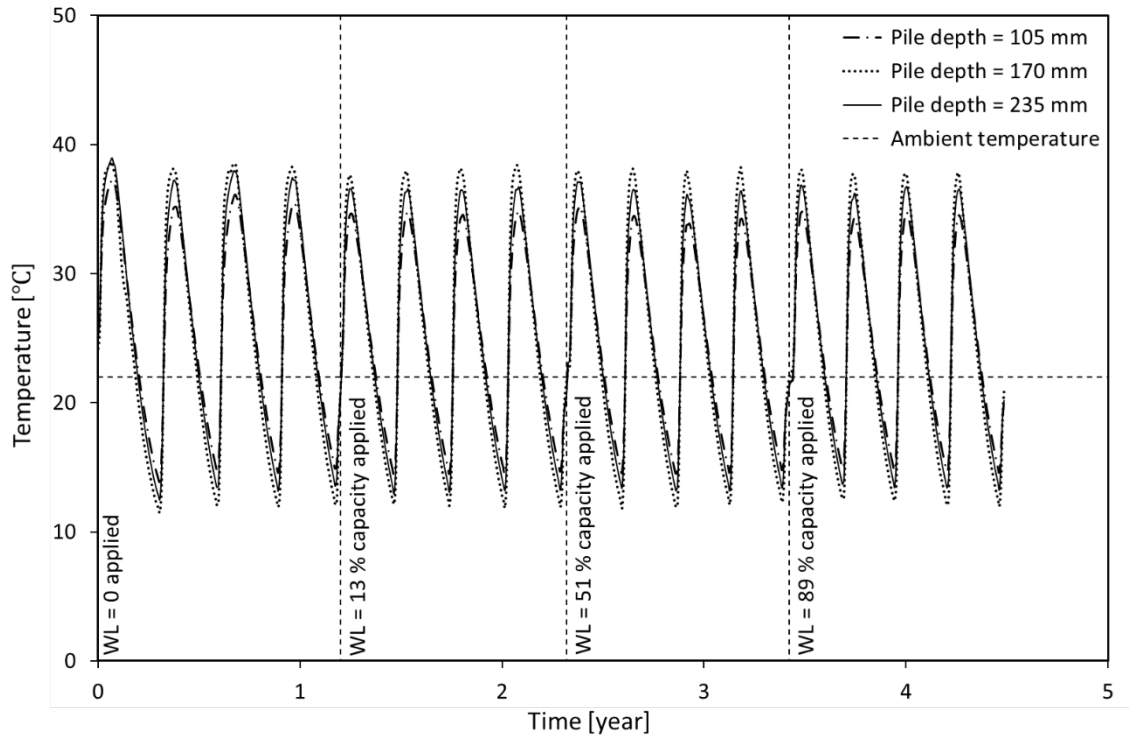
Temperature [°C]
Time [year]
Pile depth = 105 mm
Pile depth = 170 mm
Pile depth = 235 mm
Ambient temperature
WL = 0 applied
WL = 13 % capacity applied
WL = 51 % capacity applied
WL = 89 % capacity applied

(b)

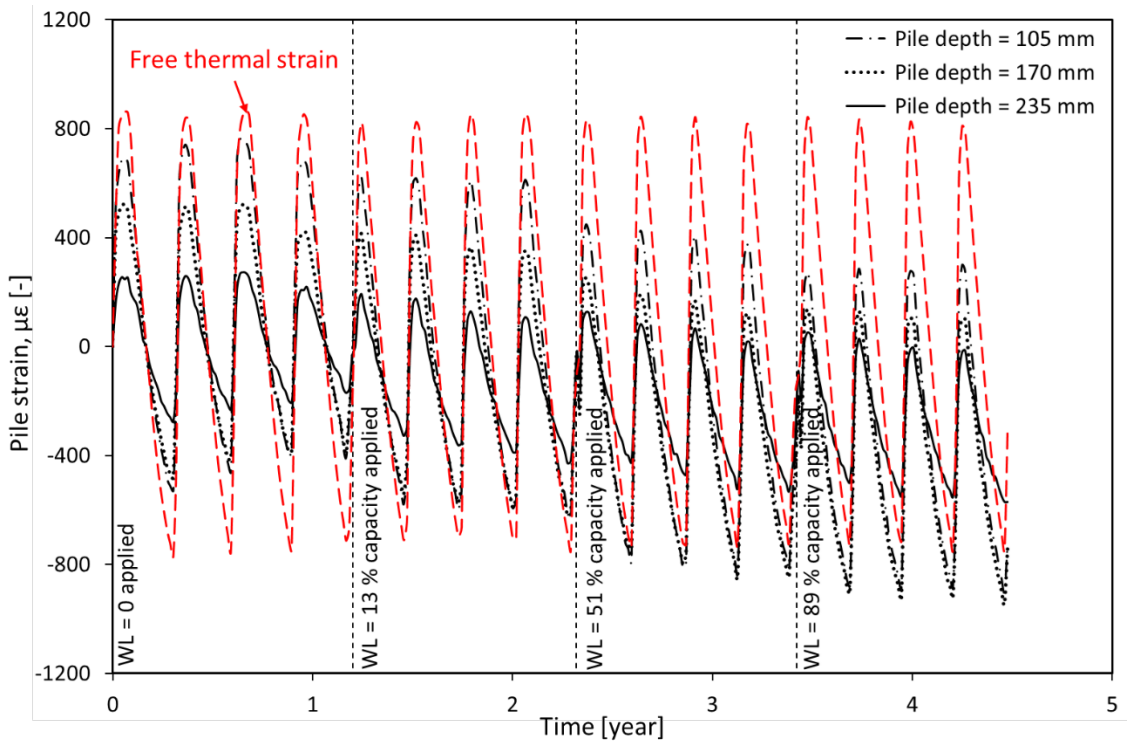


(c)

Figure 8. Time histories of (a) applied vertical load, (b) pile surface temperature and (c) thermally-induced axial strain of the model pile types 1 when subjected to cyclic pile thermal loading under maintained working loads (WL), all expressed in prototype scale following $N$ = 35 and using the 1-g scaling factors in Table 1.

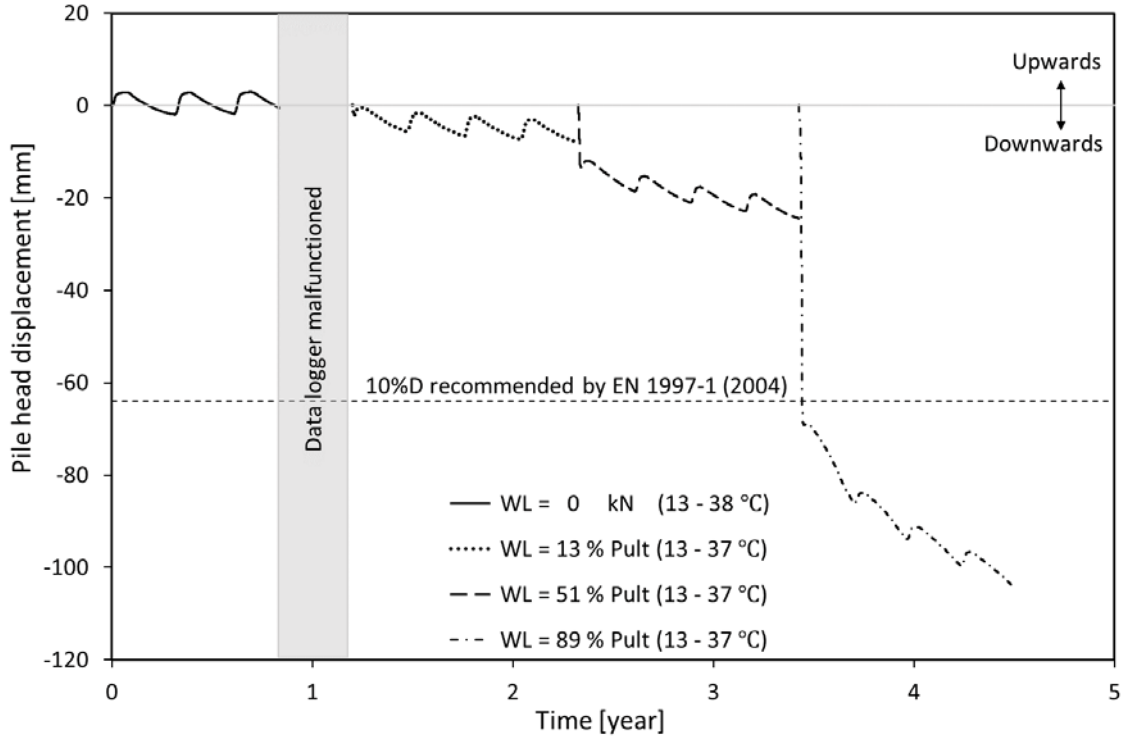


Figure 9. Pile head displacement when subjected to cyclic pile thermal loading under maintained working loads (WL), all expressed in prototype scale following *N* = 35 and using the 1-g scaling factors in Table 1.